International Journal of Coal Geology 147–148 (2015) 35–45

Contents lists available at ScienceDirect

International Journal of Coal Geology

journal homepage: www.elsevier.com/locate/ijcoalgeo

Coupled 3-D numerical simulation of proppant distribution and hydraulic fracturing performance optimization in Marcellus shale reservoirs

B. Kong, E. Fathi *, S. Ameri

West Virginia University, United States

ARTICLE INFO

Article history:
Received 19 March 2015
Received in revised form 15 June 2015
Accepted 16 June 2015
Available online 17 June 2015

Keywords:
Marcellus shale reservoirs
Hydraulic fracturing
Proppant distribution
Numerical reservoir simulation

ABSTRACT

Effective hydraulic fracturing stimulation is highly reliant on the flow area and proppant pack permeability of the induced hydraulic fractures. The flow area is largely determined by proppant distribution while fracture permeability is mainly governed by proppant sizes. To create a fracture with a large flow area, small proppants are essential to maintain a minimum proppant settling velocity; on the other hand, large proppant sizes provide higher proppant pack permeability. Therefore, an optimum operational procedure, i.e., scheduling of injection rate, proppant size and volume, is required to achieve maximum well productivity index. This, however, requires both field experiments (e.g., small volume pre-job tests) and an advanced numerical simulator that couples solid and fluid transport with fracture propagation model including mass exchange between reservoir matrix and hydraulic fracture, i.e., leak-off rate.

In this study, we focused on developing new modules for our in-house 3-D numerical simulator where proppant transport and reservoir performance optimization is considered. In new module Navier–Stokes equation describing fluid flow in the fracture and leak-off in the formation is coupled with mass conservation equation governing the proppant transport, and solved using finite difference approach. Fracture propagation is also one-way coupled with proppant transport and fluid flow using in-house 3D hydraulic fracturing simulator "HFWVU". During the simulation Proppant slippage velocity is considered over wide range of hydraulic fracturing propagation regimes, i.e., toughness-dominated to viscosity-dominated cases, with small and large leak-offs.

The simulation results predict that reservoir matrix permeability highly impacts the proppant size selection and pumping scheduling to achieve the optimum reservoir stimulation performance. Ignoring the fluid–solid interaction, i.e., proppant settling velocity, in hydraulic fracturing simulation leads to overestimating the efficiency of the process in wide range of operation conditions. It has also been predicted that the optimum combination of proppant size and their volume portion exists for specific reservoir and treatment conditions that can optimize fracture performance.

Uncertainty analysis of the reservoir behavior using experimental design technique shows that hydraulic fracturing efficiency on production performance can be highly influenced by reservoir matrix permeability, i.e., uncontrollable variable. This implies that the same hydraulic fracturing procedure applied in conventional reservoirs might not be as efficient in unconventional reservoir and special attention to reservoir characteristics needs to be made while designing the hydraulic fracturing procedure. Followed by reservoir matrix permeability, proppant volume and relative proppant/fluid density have the highest impact on hydraulic fracturing efficiency. This study couples hydraulic fracturing simulation with reservoir simulation and is a unique approach for the further understanding of proppant transport and settling, fracture geometry variation and fracture production performance. It also provides foundation for the development of sound numerical models for hydraulic fracturing design.

1. Introduction

Hydraulic fracturing has now been broadly used in petroleum industry to enhance hydrocarbon production especially in ultra-tight formations such as shale gas reservoirs. In order to produce trapped gas from underground formation, significant amount of fracturing fluid, i.e., mixture of liquid (usually water), acid, friction reducer and proppant, will be pumped into the wells at very high pressure leading to fracture propagation into the formation. When expected fracture length is achieved, the injection stops and fracturing fluid will be produced "flow back". Injected proppant will prop the fracture open against overburden pressure after flow back and provides high-conductive pathway for gas to flow from the reservoir to the wellbore. Hydraulic fracturing greatly increases the flow area and makes it economically viable to develop low porosity, low permeability reservoirs. The performance of hydraulic fracturing stimulation highly depends on proppant distribution inside the fracture. While significant

* Corresponding author.
E-mail address: ebfathi@mail.wvu.edu (E. Fathi).

http://dx.doi.org/10.1016/j.coal.2015.06.006
0166-5162/

effort has been put on simulation of fracture propagation and fluid flow during injection (CE, 1973; Cleary and Fonseca, 1992; Mobbs and Hammond, 2001; Yamamoto et al., 1999), there are not so many studies on fracture geometry after flow back. Fracture geometry after flow back is a function of proppant distribution and closure stress and is significantly different than fracture geometry after injection stops. Unwin and Hammond, 1995 and Cleary and Fonseca, 1992, included the proppant motion in vertical direction during hydraulic fracturing. Their studies show that in most cases, convection dominates proppant vertical motion over settling. Convection is affected by fracture width, density heterogeneity and fluid viscosity, while settling is mainly controlled by particle size, density ratio of solid and fluid and influenced by different hinder factors such as proppant volumetric concentration and fluid viscosity.

Commonly, the governing equations for proppant mass conservation is not coupled with fluid flow and fracture propagation equations, instead proppant effect is considered in flow equations by empirical corrections to the fluid viscosity and density (Meyer, 1986; Shah, 1980), that leads to uniform proppant distribution in the fracture. However, proppant distribution in hydraulic fractures is a strong function of different factors, including injection rate and volume, proppant size, volume and density, fracture width and also fracturing fluid viscosity and density. Quantitative analysis of the effect of each parameter and their correlations on proppant transport and distribution in fractures is vital for optimum hydraulic fracturing design.

In this study, a coupled 3-D numerical model is developed to simulate the process of proppant transport and placement during hydraulic fracturing process, the final fracture geometry after flow back is then used to estimate well productivity index. Unlike conventional approach in simulation of hydraulic fracturing that assumes uniform fluid injection (Daneshy, 1978b; Mobbs and Hammond, 2001), here point injection resembling well perforation is used capturing the physics of the process. Governing equations describing the fluid flow and leak-off and proppant motion in hydraulic fracture is coupled and to avoid checkerboard solution, staggered grid system is adopted. This is a simple way to avoid oscillatory spurious solutions when we have variables appearing as first derivatives especially in pressure velocity couplings. For the slip velocity between proppant and fluid, only gravity induced settling is considered. The hydraulic fracture represents the pseudo-3D flow domain where fracture length and height dimensions are significantly larger than its width dimension. Therefore, the variation of proppant concentration in width direction is neglected. This model handles a wide range of Newtonian and non-Newtonian fluids with different viscosity and density, and considers different injection rates, initial fracture geometry and different proppant size, density and pump scheduling. For each case proppant settling pattern is obtained and compared for sensitivity and uncertainty analysis purposes.

Finally, a single-phase fluid flow from the reservoir matrix through hydraulic fracture, to the wellbore is developed. This model is used to calculate the well productivity index as an indication of the hydraulic fracturing performance. Experimental design technique "Plackett–Burman" is also used to perform the sensitivity analysis quantifying the impact of different parameters and their relation on efficiency of hydraulic fracturing stimulation. Plackett–Burman design (PB) is a two-level factorial experiment design that allows us to investigate a large number of factors inexpensively (Rekab and Shaikh, 2005). They are generally used with eight or more (up to 47) factors where main effects have complicated confounding relationship with two-factor interactions (D. C., 2012).

2. Marcellus shale geomechanical model

The Marcellus shale in the Appalachian Basin is targeted for our study where well logs from 7 wells, core data from two wells and seismic survey are provided and used to build the 3D geomechanical model. Core data provided includes mechanical test data including mean stress, Young's modulus, Poisson ratio, shear modulus and petrophysical data including density, porosity, saturation of gas oil and water, and permeability. Fig. 1 left shows the stratigraphic structure of the area of investigation (Matthew and Carr, 2009; Milici and Swezey, 2006–1237). We have included the upper Hamilton shale and Lower Onondaga limestone in our model to be able to investigate the possible impact of hydraulic

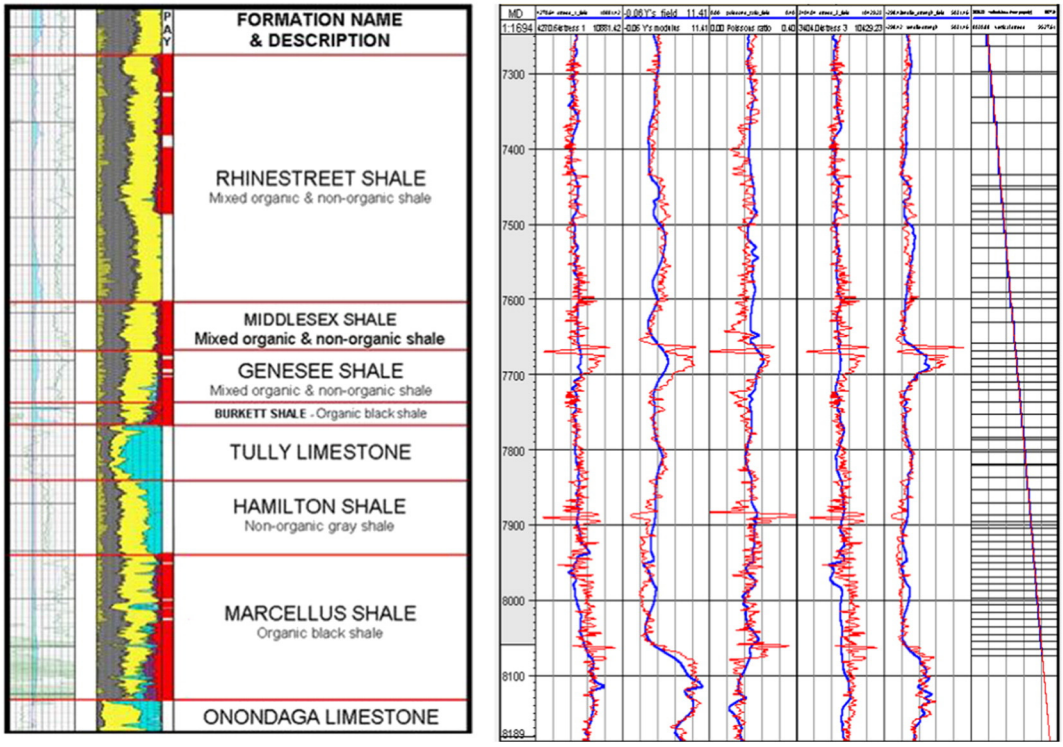

Fig. 1. Left: Stratigraphic structure of the formations, right: comparison of original log data and neural network results, from left to right, maximum horizontal stress, Young's modulus, Poisson ratio, minimum horizontal stress, tensile strength and vertical.

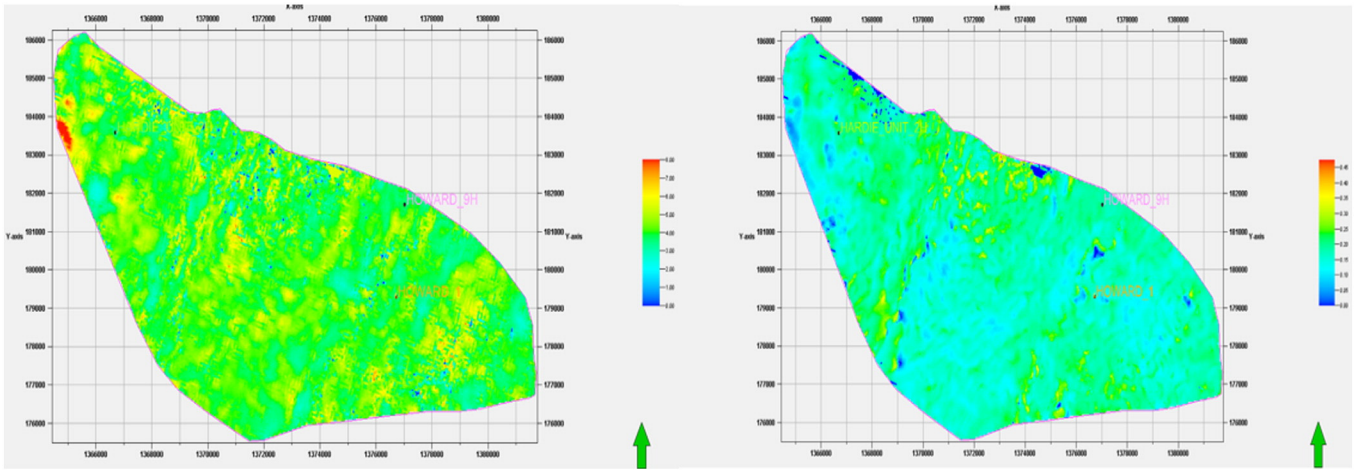

Fig. 2. Left Young's modulus and right Poisson ratio maps in horizontal well plain.

fracturing in Marcellus on upper and lower layers. Artificial Neural Network analysis is conducted using Schlumberger Petrel E&P Software Platform different seismic attributes as inputs and geomechanical properties including principle stresses, Young's modulus, Poisson ratio and tensile stress as targets. The Artificial Neural Network analysis model is first trained using half of the available geomechanical logging data and then 3-D geomechanical model is generated using the trained model. The rest of the geomechanical logging is used for quality control, which is illustrated in Fig. 1 right. Different geomechanical properties on the Marcellus shale plane which has the same depth as the horizontal parts of the wells are shown in Fig. 2 and Fig. 3. The 3-D view of Poisson ratio of formations from the Middlesex shale to Marcellus shale is shown in Fig. 4 as an example of models used as inputs for our HFWVU-3D to simulate single and multiple-fracture propagation in heterogeneous Marcellus shale formation.

3. Theories and numerical implementation

3.1. Formulation of fluid flow in hydraulic fractures

Velocity and pressure fields for an incompressible fracturing fluid can be obtained solving Navier–Stokes equations using finite difference technique. Under the assumption of constant density, mass and momentum governing equations can be simplified as follows:

$$\frac{\partial v_x}{\partial x}+\frac{\partial v_y}{\partial y}=0 \tag{1}$$

$$\frac{\partial v_x}{\partial t}+\frac{\partial P}{\partial x}=-\frac{\partial (v_x{}^2)}{\partial x}-\frac{\partial (v_x v_y)}{\partial y}+\frac{1}{Re}\left(\frac{\partial^2 v_x}{\partial x^2}+\frac{\partial^2 v_x}{\partial y^2}\right) \tag{2}$$

$$\frac{\partial v_y}{\partial t}+\frac{\partial P}{\partial y}=-\frac{\partial (v_x v_y)}{\partial x}-\frac{\partial (v_y{}^2)}{\partial y}+\frac{1}{Re}\left(\frac{\partial^2 v_y}{\partial x^2}+\frac{\partial^2 v_y}{\partial y^2}\right). \tag{3}$$

The mass conservation equation is time-independent for incompressible flow that makes it an additional constraint for the momentum conservation equation. To capture the dynamics of flow, a commonly used projection method is preferred to solve discrete equations. The key advantage of the projection method is to decouple velocity and the pressure fields. Nonlinear convection, viscous diffusion and pressure correction can be calculated in three steps: I) Solve the momentum equation for intermediate velocity field without explicit pressure variation, then II) solve pressure Poisson equation based on intermediate velocity field and III) update the intermediate velocity field using pressure gradient.

3.2. Proppant transport in hydraulic fractures

Proppant pumped in vertical hydraulic fractures mainly moves in two directions, horizontal and vertical. Horizontal movement along fracture length follows fluid flow in horizontal direction where no slippage between proppant and fluid is concerned. Horizontal movement of proppants in fracture width direction is usually negligible due to the small scale of the fracture width compared to fracture length and height. Vertical motion of proppants, however, is induced by fluid flow in vertical direction and gravity forces. Vertical velocity of proppant is referred

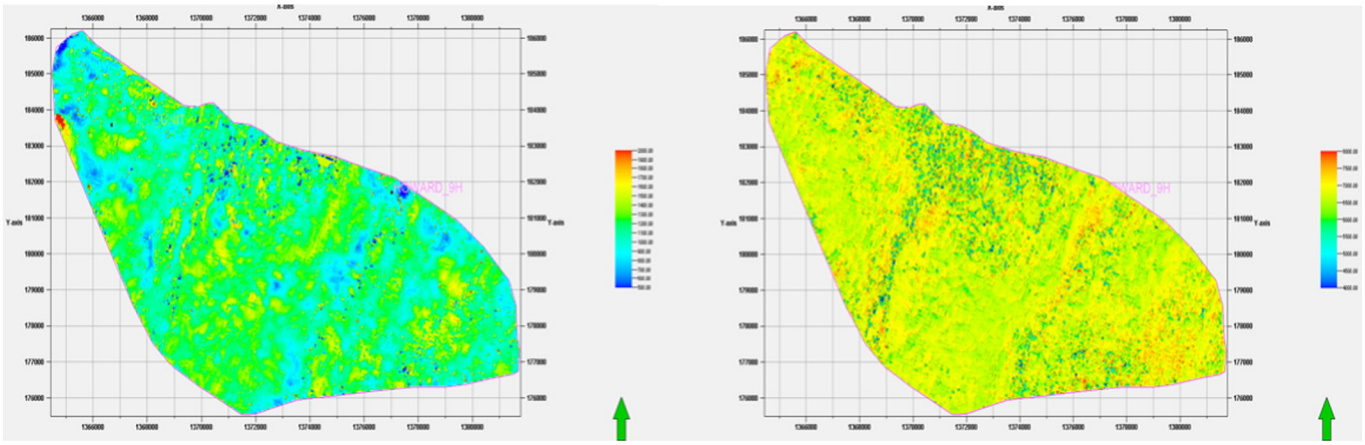

Fig. 3. Left tensile stress and right minimum horizontal stress maps in horizontal well plain.

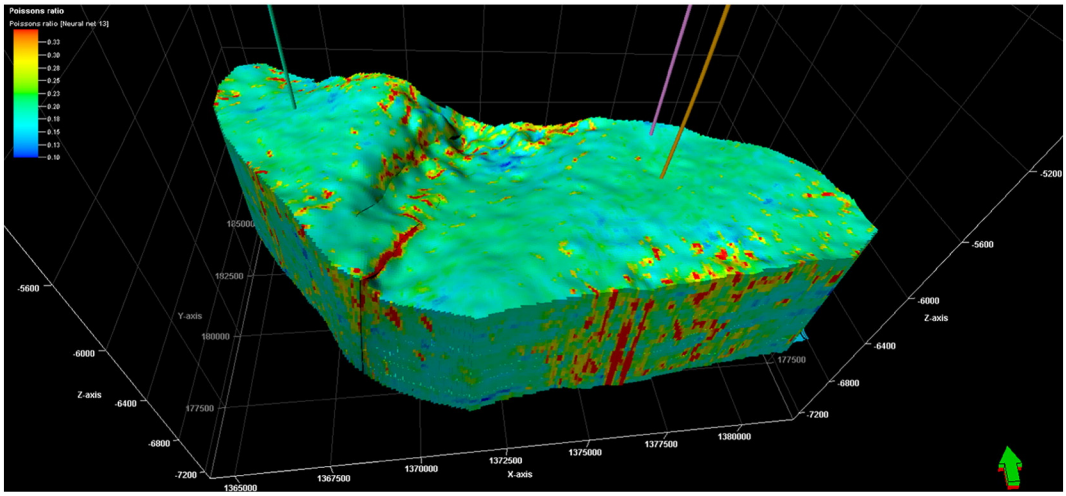

Fig. 4. 3-D view of Poisson ratio covering the Middlesex shale to Marcellus shale.

as settling velocity and is influenced by fracturing fluid properties (density and viscosity), solid properties (proppant size and density) and fracture geometry. Proppant settling stops when the proppant concentration in the slurry reaches to the maximum value beyond which it cannot move, or the fracture width becomes so small that proppant particles stuck by fracture walls due to proppant particles form a bank filling the fracture (Novotny, 1977). Therefore, the proppant velocity in x (horizontal) and y (vertical) directions can be written as follows:

$$v_x^p = v_x \tag{4}$$

$$v_y^p = v_y + v_{settle}. \tag{5}$$

The governing equation for proppant concentration is:

$$\frac{\partial c v_y^p}{\partial y} + \frac{\partial c v_x^p}{\partial x} = \frac{\partial c}{\partial t} \tag{6}$$

where v_x^p and v_y^p are proppant velocity in horizontal and vertical directions respectively, v_x and v_y are fluid velocity, v_{settle} is proppant settling velocity induced by gravity, and c is the proppant concentration by volume.

Settling velocity can be calculated using Stokes law, which describes a single spherical particle settling in an infinitely large environment (Novotny, 1977). The following equation holds when Reynolds number is less than 2:

$$V_\infty = \frac{g(\rho_p - \rho_f) d_p^{\,2}}{18\mu}. \tag{7}$$

For 2 < Re < 500 Eq. 7 changes to:

$$V_\infty = \frac{20.34(\rho_p - \rho_f)^{0.71} d_p^{1.14}}{\rho_f^{0.29}\mu^{0.43}}. \tag{8}$$

And for Re ≥ 500 Eq. 9 described the proppant settling velocity as follows:

$$V_\infty = 1.74\sqrt{\frac{g(\rho_p - \rho_f) d_p}{\rho_f}} \tag{9}$$

where ρ_p is proppant density, ρ_f is fracturing fluid density, d_p is proppant particle diameter, and μ is fluid viscosity, V_∞ is the falling velocity of a single particle in an infinitely large environment. Settling velocity of proppant can be obtained applying the polynomial correlation to V_∞ that includes the effect of proppant concentration (interaction between proppant particles) and fracture width. In this study, correction introduced by Gadde et al., 2004 is applied in two steps to obtain settling velocity in Eq. 12 (Gadde et al., 2004).

$$V_w = V_\infty \left[0.563\left(\frac{d_p}{w}\right)^2 - 1.563\left(\frac{d_p}{w}\right) + 1\right] \tag{10}$$

where V_w is settling velocity corrected for fracture wall effect, V_∞ is uncorrected settling velocity, d_p is proppant particle diameter, and w is fracture width.

$$V_c = V_\infty(2.37c^2 - 3.08c + 1) \tag{11}$$

where V_c is the settling velocity corrected for proppant concentration effect, V_∞ is uncorrected settling velocity, and c is proppant concentration. Fluid viscosity also needs to be corrected as follows:

$$\mu = \mu_0\left\{1 + \left[0.75(e^{1.5n} - 1)e^{-\frac{\gamma(1-n)}{1000}}\right]\frac{1.25c}{1 - 1.5c}\right\}^2. \tag{12}$$

Finally, the corrected settling velocity can be obtained as:

$$v_{settle} = V_\infty\left[0.563\left(\frac{d_p}{w}\right)^2 - 1.563\left(\frac{d_p}{w}\right) + 1\right](2.37c^2 - 3.08c + 1). \tag{13}$$

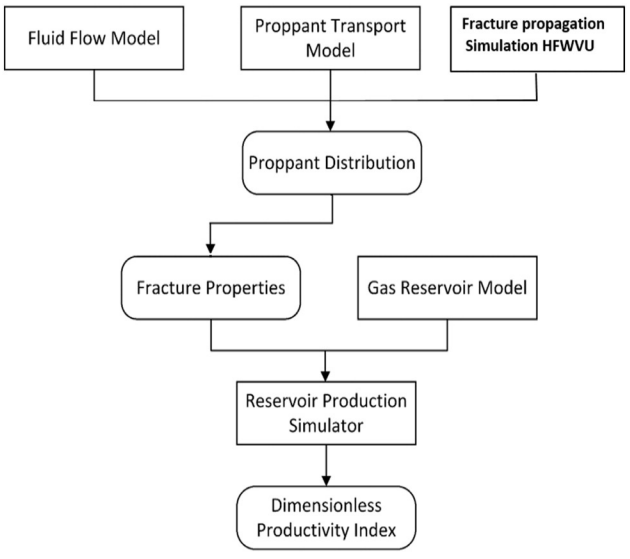

Fig. 5. Flow chart of this research.

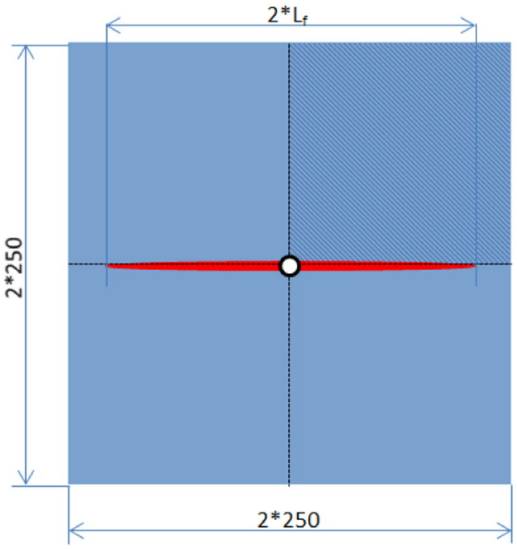

Fig. 6. Overlook of the gas reservoir model for simulation.

3.3. Fracture geometry and permeability

Different hydraulic fracturing models have been developed to study the nonlocal relationship between the net pressure in the fracture and fracture width and non-linear relationship between the fluid flow in the fracture and fracture width including the plane strain (Geertsma and Klerk, 1969), PKN (Nordren, 1972), and axisymmetric penny-shaped models (Abe et al., 1976). In this paper, an in-house numerical simulator (HFWVU) based on PKN model and the finite element method is used to simulate hydraulic fracturing in a unified way where no additional effort is needed to track the fluid front explicitly when a fluid lag exists or occurs (Bao et al., 2014a; Bao et al., 2014b). The simulation results of HFWVU have been confirmed with asymptotic solutions in different hydraulic fracturing regimes (Bao et al., 2014b). After expected hydraulic fracture length is achieved injection stops and fracturing fluid will be produced during the flow-back process and fracture starts closing up due to overburden pressure. This process increases the proppant concentration till it reaches a maximum value depending on the proppant distribution during injection period and stops the fracture walls from closing the fracture. The maximum proppant concentration required to stop closing the fracture is around 0.634, assuming that the proppant particles are perfect spheres and considering irregular sphere packing theory (Song et al., 2008). This is also verified by experimental studies using different proppant sizes. Experimental studies show that fracture width can be reduced by about 16% from 0 closure stress to 8000 psi closure stress (Barree and Conway, 1995). The fracture width at 0 closure stress"$w_f^{'}$" can be obtained using proppant concentration and original fracture width after injection as follows:

$$w_f^{'} = \mathrm{w}\,\frac{\mathrm{c}}{\mathrm{c_{max}}} \tag{14}$$

where, w is original fracture width after injection, c is proppant concentration and c_{max} is maximum proppant concentration. Based on this equation the area where proppant concentration reaches the maximum value will hold the original fracture width, while the area where proppant concentration doesn't reach the maximum value will have smaller fracture width. The proppant pack permeability, k_f, can be theoretically estimated in terms of the proppant diameter, d_p, porosity, $\varnothing$, proppant sphericity, Φ, propped fracture width, w, and damage factor, DF, using the equation given below (Bird et al., 2007)

$$\mathrm{k_f} = \frac{\varnothing^3(\mathrm{d_p}\Phi)^2}{72\lambda_\mathrm{m}\left(1-\varnothing^2\right)}\left(1+\frac{\mathrm{d_p}\Phi}{3(1-\varnothing)\mathrm{w}}\right)^{-2}(1-\mathrm{DF}) \tag{15}$$

where $\lambda_m \approx 25/12$ for most of the porosity ranges in hydraulic fractures.While studies did confirm that closure pressure can crush proppant particles or embed proppant particles into fracture walls, which will lead to a reduction of proppant pack permeability, it is also shown that this effect can be ignored when the closure pressure is under 4000 psi (Borujeni et al., 2014).

3.4. Fluid flow during production

During the gas production from the hydraulically fractured reservoir, single-phase gas flow in proppant pack is governed with similar mass and momentum conservation equations that govern fluid flow in porous media. In this case to account for non-Darcy flow effect Forchheimer equation can be used as follows:

$$\frac{1}{k_{app}} = \frac{1}{k} + 3.238 * 10^{-8}\frac{\rho\beta\nu}{\mu} \tag{16}$$

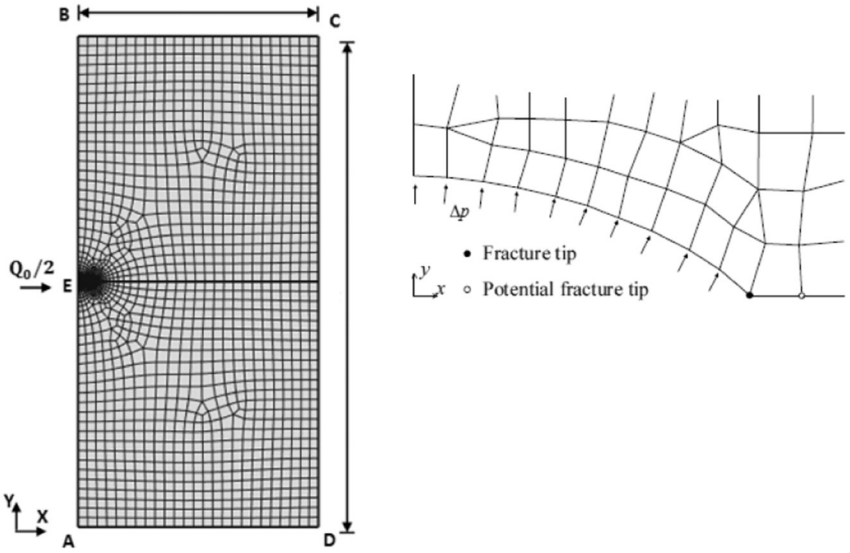

Fig. 7. (a) Single fracture propagation model with 100 elements (HFWVU) and (b) discretization of the equivalent quarter model with finite elements in HFWVU.

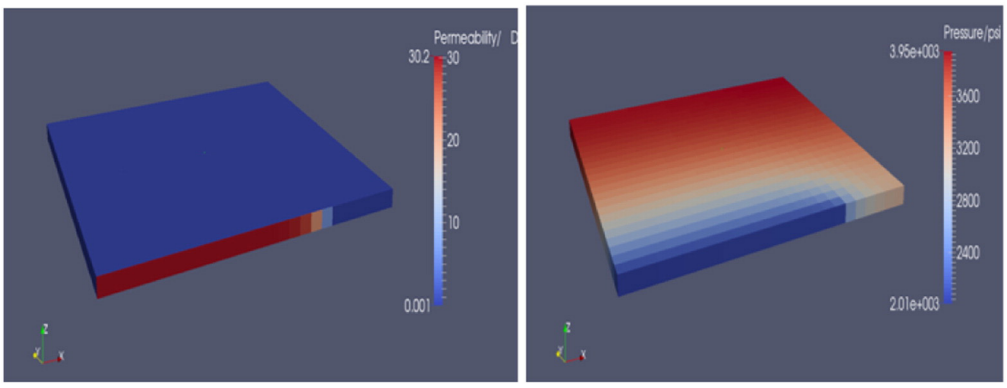

Fig. 8. Permeability (left) and pressure (right) distribution in reservoir and hydraulic fracture, considering zero proppant settling velocity.

where β is non-Darcy factor or Forchheimer factor and k_{app} is the apparent permeability. Following correlation can be used to calculate non-Darcy factor (Armenta and Wojtanowicz, 2013)

$$\beta = 1.88 * 10^{10} k^{-1.47} \varnothing^{-0.53}. \tag{17}$$

The governing equation of compressible fluid flow in porous media can be written as: (Ertekin et al., 2001)

$$\frac{\partial}{\partial x}\left(\frac{k_x A_x}{\mu B}\frac{\partial \Phi}{\partial x}\right)\Delta x + \frac{\partial}{\partial y}\left(\frac{k_y A_y}{\mu B}\frac{\partial \Phi}{\partial y}\right)\Delta y + \frac{\partial}{\partial z}\left(\frac{k_z A_z}{\mu B}\frac{\partial \Phi}{\partial z}\right)\Delta z + q = v_b \frac{\partial}{\partial t}\left(\frac{\varnothing}{B}\right). \tag{18}$$

3.5. Hydraulic fracturing performance evaluation

In this paper, first the proppant distribution in a single hydraulic fracture is obtained and then hydraulic fracture geometry and fracture permeability after flow back is calculated. The simulation results of hydraulic fracture geometry and permeability after the flow back are then used in a fractured reservoir model for hydraulic fracturing performance optimization. Here, the dimensionless productivity index "*I*" is employed to compare the performance of different hydraulic fracturing operations.

$$I = J_a / J_b \tag{19}$$

where J_a is the productivity index after stimulation and J_b is the productivity before stimulation, where the productivity index for gas reservoir is defined as (Pearson, 2001):

$$J_g = \frac{q\mu z}{\bar{p}_r^2 - p_{wf}^2} \tag{20}$$

where J_g is the productivity index of gas reservoir, z is the gas compressibility factor, μ is the gas viscosity, q is the gas flow rate in standard conditions, $\bar{p}_r$ is the reservoir average pressure, and p_{wf} is the flowing bottom hole pressure. Fig. 5 shows the flow chart that we followed to deliver this study.

Fig. 6 illustrates the schematic of the hydraulically fractured reservoir model that is a $500 * 500 * 10$ ft^3 reservoir with a producer located at the center of the reservoir. Fig. 7 shows the discretization of the equivalent half model with finite elements in HFWVU simulator. Symmetric behavior is assumed, therefore, reservoir performance analysis will be performed on a quarter of the entire model. The range of proppant size is very important. Typical proppant sizes are generally between 8 and 140 mesh (106 μm–2.36 mm), including 16–30 mesh (600 μm–1180 μm), 20–40 mesh (420 μm–840 μm), 30–50 mesh (300 μm–600 μm), 40–70 mesh (212 μm–420 μm) and 70–140 mesh (106 μm–212 μm). When describing frac sand, the product is frequently referred to as simply the sieve cut, e.g. 20/40 sand. The range of proppant size used here is a typical proppant size, i.e., 0.1–0.8 mm. For the base case the proppant size of 0.6 mm, i.e., 20/40 mesh, and reservoir permeability of 100 nano-Darcy is assumed with maximum fracture half-length of 200 ft.

4. Results and discussion

The effect of Proppant transport and settling on pressure and permeability distributions in a single hydraulic fracture in Marcellus shale gas reservoir is investigated and compared with commonly used uniform proppant distribution models. The effects on efficiency of hydraulic fracturing stimulation in different cases is compared using dimensionless productivity index of the hydraulically fractured reservoir. Next, the effect of injecting different proppant sizes and volumes for different reservoir permeability and initial fracture geometries is studied and

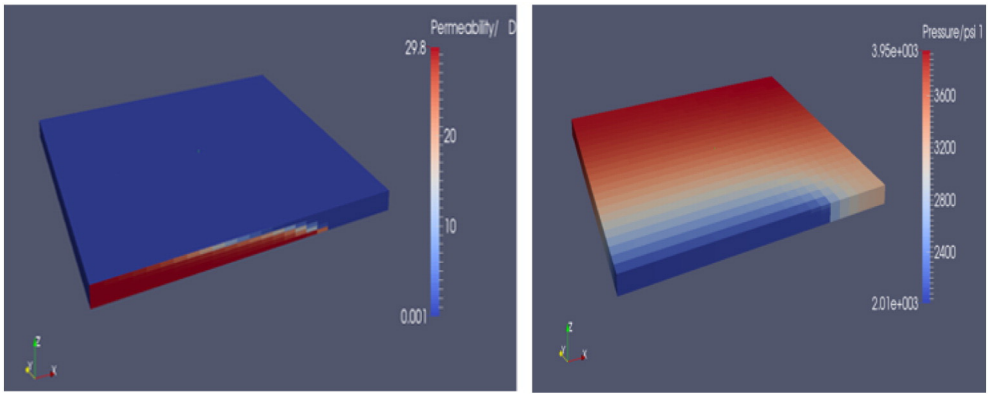

Fig. 9. Permeability (left) and pressure (right) distribution in reservoir and hydraulic fracture, considering dynamic proppant settling velocity.

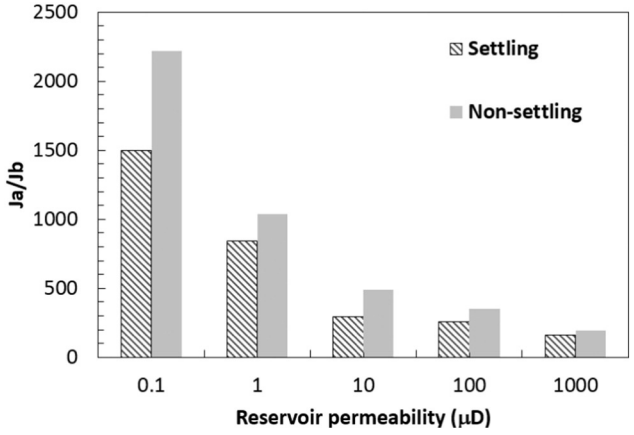

Fig. 10. Influence of proproppant settling on dimensionless productivity index, the proppant size is 0.8 mm.

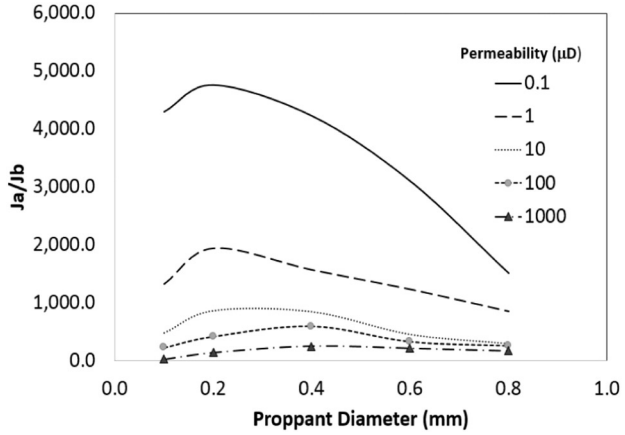

Fig. 11. The effect of proppant size on dimensionless productivity for different permeability reservoir.

multi-proppant size combination treatment for maximum stimulation efficiency is obtained for a specific set of reservoir parameters. Systematic approach based on design of experiments has been used to determine the most important parameters and their correlations impacting the hydraulic fracturing stimulation performance. Multi-proppant size combination treatment is also optimized.

4.1. Effect of non-Darcian flow, proppant settling velocity, proppant size and relative density on stimulation performance

If proppant settling velocity during the injection period is not considered, the proppant will distribute uniformly in the hydraulic fracture and results in a uniform distribution of hydraulic fracture permeability as shown in Fig. 8 (left). Pressure distribution after 2 days in the hydraulic fracture and reservoir matrix are also shown in Fig. 8 (right). Considering the fluid–rock interactions, however, leads to dynamic proppant settling velocity causing non-uniform proppant distribution along the hydraulic fracture, as clearly illustrated in Fig. 9 (left). Pressure distribution after 2 days of gas production in the reservoir matrix and hydraulic fracture can also be obtained, Fig. 9 (right).

In Fig. 10 the effect of proppant settling velocity on hydraulic fracturing performance is investigated using dimensionless productivity index for the base case model described in Table 1. The simulation results show that ignoring the effect of proppant settling leads to more than 18.6% overestimation on dimensionless productivity index, i.e., the ratio of productivity index after and before stimulation, and therefore hydraulic fracturing stimulation efficiency. Decreasing the reservoir matrix permeability or increasing the proppant size pronounces the effect by 32.4% overestimation. Larger proppant size leads to much better proppant pack permeability, however, that increases the proppant settling velocity and creates early proppant banks that reduce propped area. Therefore it's critical to find the optimum proppant size that leads to the best combination of proppant pack permeability and propped area leading to higher productivity index of the fracture for a given set of parameters defined in Table 1. Fig. 11 clearly shows that the proppant size has different impacts on stimulation performance depending on the shale matrix permeability. In high permeability formations, i.e., K > 100 μD for the sets of parameters defined in Table 1, injecting larger proppant size leads to higher productivity index, for intermediate shale matrix permeability, i.e., 1 μD < K < 100 μD, injecting larger proppant size leads to higher productivity index, however, the productivity index is not sensitive to a wide range of proppant sizes and for proppant size larger than 0.5 mm the productivity index decreases. In tight formations, i.e. k < 1 μD, critical proppant size exists that can lead to maximum stimulation efficiency, for the set of parameters presented in Table 1 the optimum proppant size turned out to be 0.2 mm. Unlike high permeability formations increasing the proppant size larger than the critical proppant size leads to decrease in productivity index and reduces the stimulation performance efficiency. The impact of optimum proppant size selection on stimulation performance pronounced in lower permeability formations such as Marcellus shale gas reservoir.

In the industry sand and resin coated sand with density of 2.65 g/cc is commonly used. Recently new application of ultra-lightweight proppant (1.25 g/cc) resin-impregnated and coated nut hull, ultra-lightweight plastic composite proppant (1.5 g/cc),light weighted ceramic, intermediate density ceramic and high density ceramic (2.72 g/cc, 3.27 g/cc, and 3.56 g/cc) is also suggested (Economides and Martin, 2007). Fig. 12 shows the impact of the relative density of proppant to fluid on stimulation performance analysis. As relative density of the proppants increases, settling velocity increases that leads to early proppant bank accumulation and decrease in propped area. This consequently

Table 1
Base case parameters.

Relative density	2.08
Proppant size	0.2 mm
Reservoir permeability	1 mD
Prop volume	0.7
Fluid viscosity	1 cp
Fracture width	0.017 ft
Injection rate	0.2 ft/s

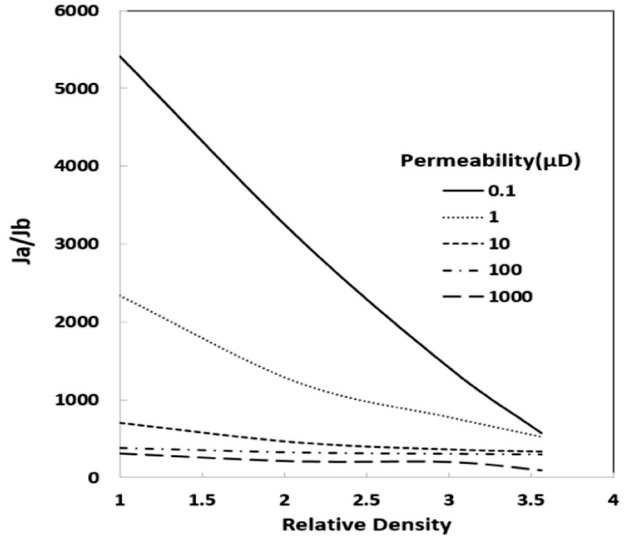

Fig. 12. The effect of relative proppant density on dimensionless productivity for different permeability reservoir.

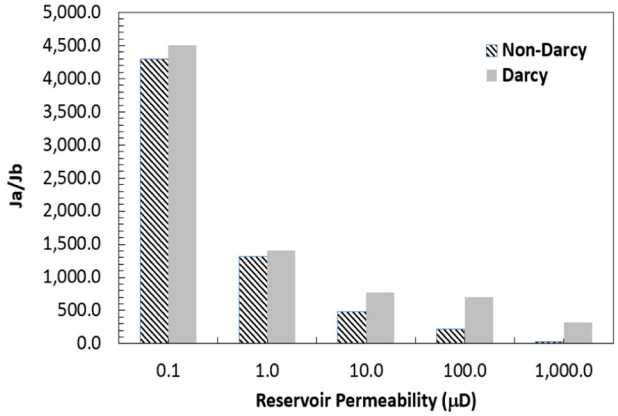

Fig. 13. Influence of non-Darcy effect on dimensionless productivity index.

decreases the stimulation performance. Fig. 12 also shows much higher stimulation efficiency drop in tighter formations such as shale gas reservoirs as a function of relative proppant density.

Fig. 13 shows the impact of non-Darcian flow in stimulation performance analysis. Ignoring the non-Darcy effect in simulation results in 4.5% overestimation of stimulation performance. The effect is more pronounced in higher matrix permeability formations as expected.

Table 2
Parameter setting of PB design.

Parameter	−1	1	unit
A: Fluid viscosity	1	10	cp
B: Proppant size	0.1	2	mm
C: Relative density	1.5	3.5	1
D: Injection rate	0.2	1	ft/s
E: Fracture width	0.017	0.2	ft
F: Permeability	0.1	100	mD
G: Prop volume	0.45	0.9	1

4.2. Proppant size combination optimization

Multi size proppant combination can maintain relatively large fracture area as well as high fracture permeability in the near wellbore region. In this section, different proppant combinations, i.e., different volume portion, relative proppant density and different proppant size combinations are simulated and their performance is compared with each other. The reservoir permeability is 0.01 μD and the smaller proppant size is 0.2 mm. A series of different larger proppant sizes and its volume portion is simulated. The results are shown in Fig. 14a, b and c. Simulation results show that larger size of the later injected proppant leads to a better performance as long as relative density of proppant are in the range of light to intermediate. However in the

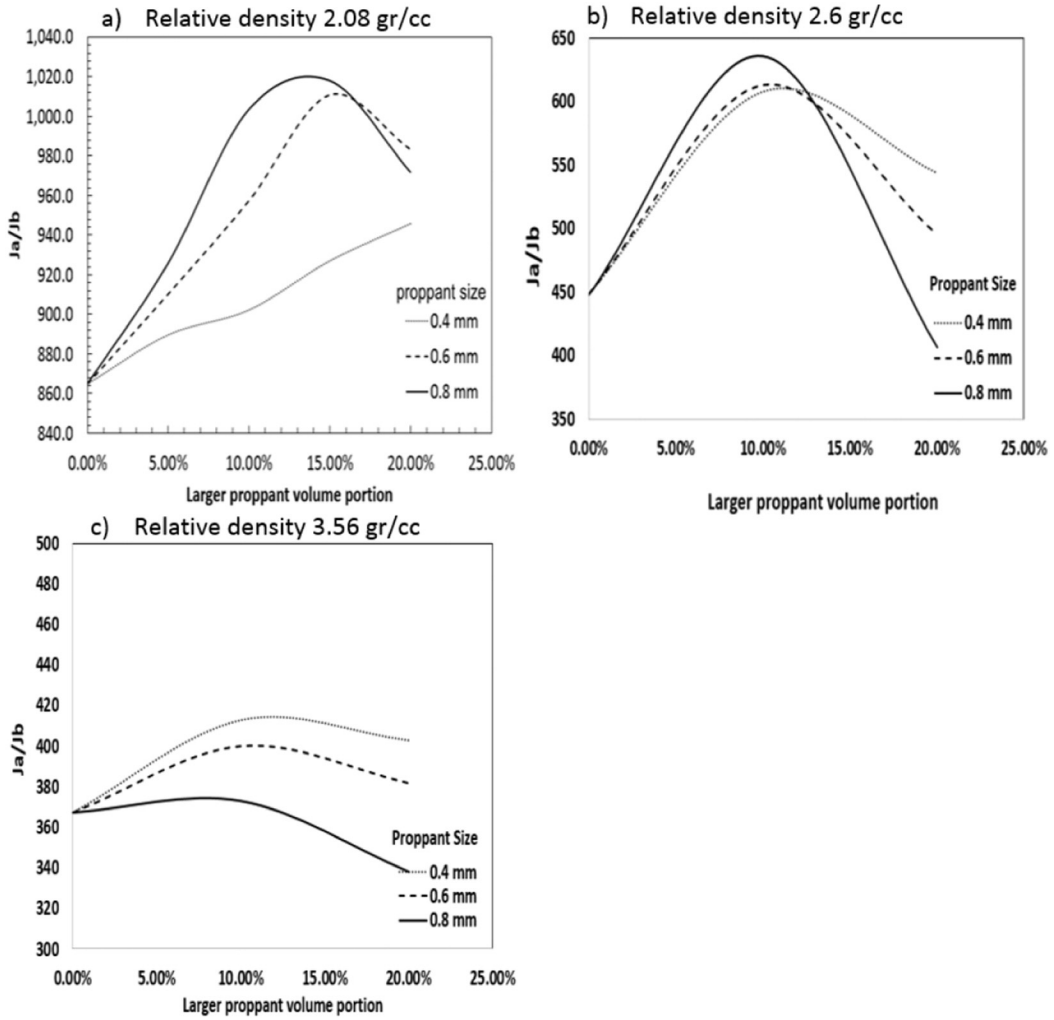

Fig. 14. The effect of proppant size and volume portion combination on dimensionless productivity.

Table 3
PB matrix for 7 variables (−1 = low value, +1 = high value).

Run	Factor 1 A: Fluid viscosity (cp)	Factor 2 B: Proppant size (mm)	Factor 3 C: Relative density (1)	Factor 4 D: Injection rate (s)	Factor 5 E: Fracture width (in)	Factor 6 F: Permeability (D)	Factor 7 G: Prop volume	Response Dimensionless PI
1	1	1	−1	1	1	−1	1	2.11E+02
2	1	1	1	−1	1	1	−1	4.15E+01
3	1	1	−1	1	−1	−1	−1	2.07E+02
4	−1	1	−1	−1	−1	1	1	1.01E+02
5	1	−1	1	−1	−1	−1	1	4.14E+02
6	1	−1	1	1	−1	1	−1	2.69E+01
7	−1	1	1	−1	1	−1	−1	2.57E+02
8	−1	1	1	1	−1	1	1	9.02E+01
9	−1	−1	−1	−1	−1	−1	−1	2.66E+02
10	−1	−1	−1	1	1	1	−1	2.72E+01
11	1	−1	−1	−1	1	1	1	2.77E+01
12	−1	−1	1	1	1	−1	1	4.12E+02

case of high density ceramics larger proppant size leads to lower hydraulic fracturing performance. Also, there exist an optimum volume portion for the later injected proppant in the range of light to intermediate proppant density, and the portion is about 10% to 15% depending on the proppant size.

4.3. Uncertainty analysis using design of experiments

For real field application of stimulation performance analysis, one needs to consider the uncertainty analysis and risk assessment using wide range of model variables impacting the process. Due to the fact that different parameters like reservoir permeability, and mechanical properties, proppant size, volume and density, injection rate and fluid viscosity contribute to the hydraulic fracture performance, it is very hard to quantify the impact of each one of these parameters using simple one variable at a time studies (OVAT). This is due to correlations that exist between different parameters impacting the hydraulic fracturing performance. In this study the Plackett–Burman (PB) experiment technique is used to quantify the contribution of each candidate parameters and their interactions on hydraulic fracturing stimulation. The PB design settings are listed in Table 2 and Table 3 (Plackett and Burman, 1946). The PB design is the most compact two-level design of resolution of III. Resolution III design does confound main effects with two-factor interactions, i.e., all main effects can be determined (D. C., 2012). In Tables 2 and 3, minimum and maximum values assigned to 7 different parameters expected to have the highest impact on hydraulic fracturing performance are presented with −1 and +1 values, respectively. In general, PB requires (n + 1) runs, where "*n*" is the number of variables but they are usually in multiples of 4.

In this research, Pareto chart, and normal plot of the standardized effects will be used for uncertainty analysis. Fig. 15 shows that reservoir permeability, proppant volume and proppant density have significant influence on the dimensionless productivity index while proppant size, fluid viscosity, injection rate and fracture width having less impact. However, one needs to consider the fact that PB design is not fully considering the two-factor interactions. In the normal probability plot of the effects (Fig. 16), points that do not fall near the line usually indicate important effects. Important effects are larger and generally further from the fitted line than unimportant effects. Unimportant effects tend to be smaller and centered on zero, these are in agreement with Fig. 15. Also, normal plot can identify the effect polarity of each variable. For example, the standard effect of reservoir permeability is negative, which means that small permeability reservoir tend to have better improvement from hydraulic fracturing treatment. Fig. 16 clearly

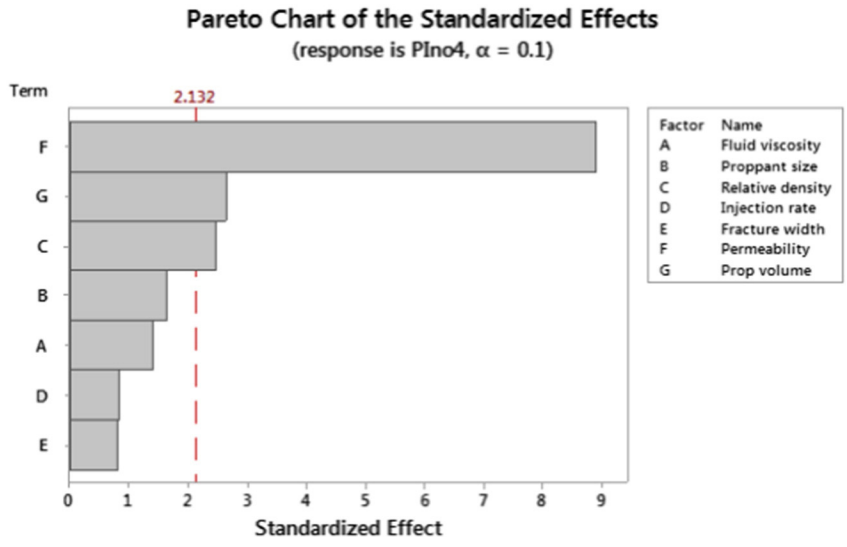

Fig. 15. Pareto chart shows the importance of parameters evaluated on the t-value of original case.

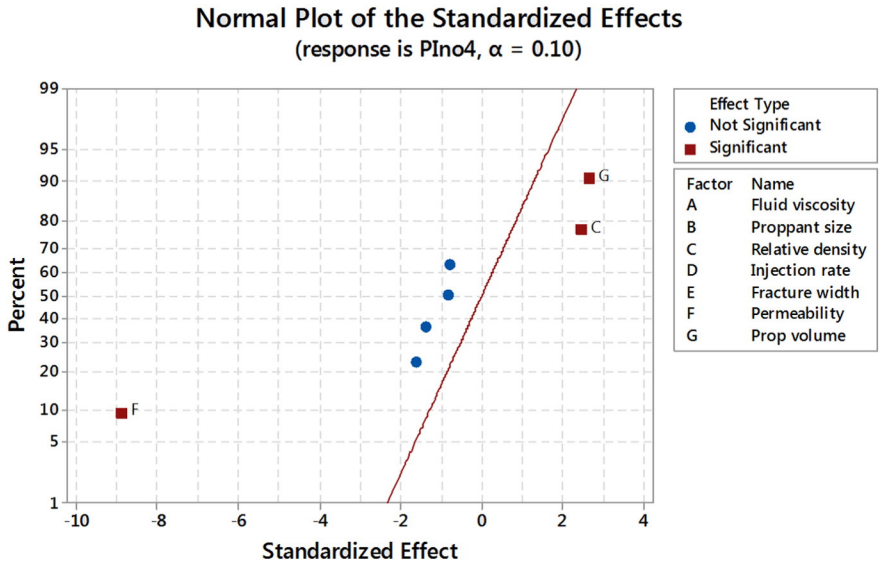

Fig. 16. Normal plot of the standardized effects of original case shows the importance of parameters.

shows that reservoir matrix permeability has the highest negative impact on simulation response and prop volume and then relative density of proppant to fracturing fluid has the highest positive impact on dimensionless productivity index. The alias structure of PB design is complex (D. C., 2012). All main effects have two-factor, three-factor and more interaction alias chains. To minimize the error, we also performed full fold-over design to eliminate the entire two-factor interaction alias from main effects.

5. Conclusion

Coupled 3-D numerical simulator is developed using Fortran 90 including three major parts: hydraulic fracture propagation model, fluid and proppant transport, hydraulic fracture geometry calculation after flow back and hydraulic fractured gas reservoir production. In this study different parameters impacting proppant-settling velocity such as non-Newtonian flow, fracture width, fracture leak-off, proppant volume, relative density, size and concentration effects are considered. In addition, sensitivity analysis is implemented to evaluate the impact of different controllable and uncontrollable parameters on dimensionless productivity index. Design of experiment technique (PB) is used to identify the magnitude and statistical significance of most important parameters impacting hydraulic fracturing stimulation.

Our study shows that proppant settling can cause heterogeneous distribution of proppant and reduce the cumulative production by 18.6% or more depending on the reservoir matrix permeability. It also predicts an optimum proppant size to achieve maximum hydraulic fracturing efficiency in tight formations such as shale with known matrix permeability as a function of relative proppant density. The Simulation results also predict that the combination of smaller proppant followed by larger proppant size can improve the stimulation performance and there exist an optimum value for larger proppant size volume injected to achieve the maximum stimulation efficiency. It also predicted that the magnitude of the difference between two proppant sizes can also significantly impact the stimulation efficiency depending on the relative proppant density.

Sensitivity analysis of proppant size while other parameters kept constant shows that in low permeability reservoir, smaller proppant size with lower relative density is generally more suited and there is an optimum proppant size exist that can reduce the settling velocity and lead to a larger flowing area; in a high permeability reservoir, however, larger proppant can provide better performance because high permeability flow channel is more granted.

Nomenclature

B	Volume fraction	Fraction
B_{gi}	Initial gas formation factor	Fraction
B_w	Water formation factor	Fraction
c	Proppant concentration by volume	Fraction
c_f	Rock compressibility	1/Pa
C_l	Carter's leak-off coefficient	$m/\sqrt{s}$
c_{max}	Maximum proppant concentration by volume	Fraction
cw	Water compressibility	1/Pa
dp	Proppant diameter	m
DF	Proppant damage factor	Fraction
JD	Dimensionless productivity	Fraction
k	Reservoir permeability	D
k_{app}	Apparent permeability	D
k_f	Fracture permeability	D
n, γ	Constant of non-Newtonian fluid	1
P	Pressure	Pa
$\overline{pr}$	Reservoir average pressure	Pa
p_{sc}	Pressure at standard condition	Pa
p_{wf}	Well flow pressure	Pa
q	Production rate	m^3/s
q_l	Leak-off velocity	m/s
R_e	Reynold's number	1
U	Fluid velocity	m/s
V_∞	Uncorrected proppant settling velocity	m/s
v_b	Bulk volume of cell	m^3
V_c	Proppant settling velocity corrected for concentration	m/s
v_{settle}	PROPPANT settling velocity	m/s
V_w	Proppant settling velocity corrected for fracture width	m/s
vx	Fluid velocity in x direction	m/s
vp	Proppant velocity	m/s
vy	Fluid velocity in y direction	m/s
w	Fracture width	m
w_f	Final fracture width after flow back	m
μ	fluid viscosity	mPa·s
μ_0	Viscosity of Newtonian fluid without proppant	mPa·s
ρ_f	Fluid density	kg/m^3
ρ_p	Proppant density	kg/m^3
ρ_{sc}	Density at standard condition	kg/m^3
Φ	Proppant sphericity	1
$\varnothing$	Porosity	Fraction

Acknowledgments

We would like to thank RPSEA's Funding (Grant/Contract No: #9122-06) for this project. RPSEA (www.rpsea.org) is a multi-purpose entity whose mission is to provide stewardship in ensuring the focused research, development and deployment of safe and environmentally responsible technology that can effectively deliver hydrocarbons from domestic resources to the citizens of the United States.

References

Abe, H., Mura, T., Keer, L., 1976. Growth-rate of a penny-shaped crack in hydraulic fracturing of rocks. J. Geophys. Res. 81 (29), 5335–5340.

Armenta, M., Wojtanowicz, a.K., Apr. 2013. Rediscovering non-Darcy flow effect in gas reservoir. SPE Annu. Tech. Conf. Exhib. 1–8.

Bao, J.Q., Fathi, E., Ameri, S., 2014a. A coupled finite element method for the numerical simulation of hydraulic fracturing with a condensation technique. Eng. Fract. Mech. 131, 269–281.

Bao, J.Q., Fathi, E., Ameri, S., 2014b. Uniform investigation of hydraulic fracturing propagation regimes in plane strain model. Int. J. Numer. Anal. Methods Geomech. http://dx.doi.org/10.1002/nag.2320)19.

Barree, R., Conway, M., 1995. Experimental and numerical modeling of convective proppant transport. JPT. J. Pet. Technol. 216–223 (no. March).

Bird, R.B., Stewart, W.E., Lightfoot, E.N., 2007. Transport Phenomena. John Wiley & Sons, p. 905.

Borujeni, A.T., Tyagi, M., White, C.D., 2014. "Effects of Stress-Dependent Hydraulic Properties of Proppant Packs on the Productivity Indices of the Hydraulically Fractured Gas Reservoirs". SPE-2014-1934187-MS, SPE/AAPG/SEG Unconventional Resources Technology Conference, 25–27 August, Denver, Colorado, USA.

CE, C., 1973. Conductivity of fracture proppants in multiple layers. J. Pet. Technol. 1101–1107.

Cleary, M.P., Fonseca Jr., Amaury, 1992. "Proppant Convection and Encapsulation in Hydraulic Fracturing: Practical l mplications of Computer and Laboratory Simulations".

D. C., May 2012. Montgomery Design and Analysis of Experiments. 8th Edition. 978-1-118-32426-4.

Daneshy, A.A., 1978. Numerical solution of sand transport in hydraulic fracturing. J. Pet. Technol. Trans. AIME. 132–140.

Economides, M.J., Martin, T., 2007. Modern Fracturing Enhancing Natural GAs Production. ET Publishing, Houston TX.

Ertekin, T., Abou-Kassem, J.H., King, G.R., 2001. Basic applied reservoir simulation. Soc. Petrol. Eng. 406.

Gadde, P., Yajun, L., Jay, N., Roger, B., Sharma, M., 2004. Modeling proppant settling in water-fracs. Proc. SPE-89875-MS, SPE Annu. Tech. Conf. Exhib, 26-29 September, Houston, Texas.

Geertsma, J., Klerk, F.d., 1969. Rapid method of predicting width and extent of hydraulically induced fractures. J. Pet. Technol. 21, 1571–1581.

Matthew, B.L., Carr, T.R., 2009. Lithostratigraphy and Petrophysics of the Devonian Marcellus Interval in West Virginia and southwestern Pennsylvanian. http://www.mapwv.gov/UnconventionalResources/marcellusLithoAndPetroPaper.pdf.

Meyer, B.R., 1986. "Generalized Drag Coefficients Applicable for All Flow Regimes," OGJ.

Milici, R.C., Swezey, C.S., 2006–1237. Assessment of Appalachian Basin oil and gas resources: Devonian shale-middle and upper Paleozoic total petroleum system. USDI & USGS Open-file Report Seriespp. 10–22.

Mobbs, A.T., Hammond, P.S., 2001. "Computer Simulations of Proppant Transport in a Hydraulic Fracture," SPE Production & Facilities. vol.16.no 2.

Nordren, R.P., 1972. Propagation of a Vertical Hydraulic Fracture. SPE 7834. 12. 8, pp. 306–314.

Novotny, E.J., 1977. Proppant Transport. SPE 6813, SPE Annu. Fall Tech. Conf. Exhib. 9-12 October, Denver, Colorado.

Pearson, C., 2001. Dimensionless fracture conductivity: better input values make better wells. J. Pet. Technol. 53 (1) January.

Plackett, R.L., Burman, J.P., June 1946. The design of optimum multifactorial experiments. Biometrika 33 (4), 305–325.

Rekab, K., Shaikh, M., 2005. Statistical Design of Experiments with Engineering Applications. Taylor & Francis Group, LLC.

Shah, S.N., 1980. "Proppant Settling Correlation for Non-Newtonian Fluids Under Static & Dynamic Conditions", paper SPE 9330.

Song, C., Wang, P., Makse, H. a, May 2008. A phase diagram for jammed matter. Nature 453 (7195), 629–632.

Unwin, A.T., Hammond, P.S., 1995. Computer Simulations of Proppant Transport in a Hydraulic Fracture SPE 29649 Western regional meeting Bakersfield, CA, U.S.A., S-10 March.

Yamamoto, K., Shimamoto, T., Maezumi, S., 1999. "Development of a True 3D Hydraulic Fracturing Simulator", SPE Asia Pacific Oil. pp. 1–10.